# Chapter 1

# Introduction

This PhD thesis treats of the prototype of a hard x-ray high resolution scanning microscope using nanofocusing refractive lenses. The scanning microscope (synonymously called "nanoprobe") was developed, built and operated by our study group in Dresden in the course of a project supported by the German Department of Education and Research (Bundesministerium für Bildung und Forschung, BMBF). The main goal of the project was to demonstrate the possibility to generate a small intense x-ray focus with a full width at half maximum size below 100 nm, which can be employed for spatially resolved x-ray analysis. In a follow-up venture, we are currently assembling an upgraded version of a hard x-ray scanning microscope to be installed at the PETRA III beamline P06, bringing in the experiences we made with the prototype version.

Hard x rays are capable of pervading matter and, therefore, x rays — in contrast to visible light, soft x rays, or electron beams — are capable of revealing the interior properties of specimens without destructive sample preparation. Since their discovery by W. C. Röntgen in 1895 [Rön95, Rön98], a large variety of x-ray analytical techniques have been developed and successfully applied. Among others, there are x-ray crystallography, x-ray reflectometry, x-ray fluorescence spectroscopy, x-ray absorption spectroscopy, small angle x-ray scattering, and grazing incidence small angle x-ray scattering. For years, these methods were performed with large (unfocused) x-ray beams, illuminating the complete sample or at least large areas of the specimen, and for this reason, these methods were insensitive to the spatial Distribution of the investigated properties. In order to retrieve the local distribution of the observed property rather than just an average over the complete object, the sample has to be scanned by a small x-ray beam. Generating small and intense x-ray beams requires highly brilliant x-ray sources and high quality focusing optics. Compared with visible light available x-ray sources are comparably weak and focusing optics quite inefficient. Thus, the generation of highly intense and small sized x-ray beams is difficult, and it was not until the advent of third generation synchrotron radiation facilities, that hard x-ray scanning microscopy has begun to emerge as a beneficial tool for sample investigations.

The hard x-ray scanning microscope makes use of nanofocusing refractive x-ray lenses made of silicon (NFLs) [SKH$^+$03, SKP$^+$05a] and of compound parabolic refractive lenses made of beryllium (CRLs) [LST$^+$99]. The NFLs provide a sub-100 nm focal spot by in-

ducing a demagnified image of the x-ray source, while the CRLs are employed as part of a prefocusing device, which adapts the transverse coherence length to the aperture of the NFL. The nanofocusing lenses are developed by our study group in Dresden, and the compound parabolic refractive lenses are manufactured in cooperation with Prof. Lengeler at the RWTH Aachen. In fact, the evolution of the hard x-ray scanning microscope and the development of the nanofocusing lenses are interdependent. The NFLs provide the focal spot which is used by the scanning microscope for sample investigation, while, as a side effect, the NFLs are additionally characterized. The characterization delivers valuable information about aberrations from the ideal lens shape, and this information is incorporated in the design and manufacturing process of improved NFLs, pushing forward the performance of the nanoprobe.

The prototype was built in Dresden, but since it requires the highly brilliance of an undulator x-ray source, it was installed at the ESRF beamline ID 13. A long-term collaboration with the beamline ID 13 offered the possibility to regularly test the instrument and to carry out a lot of experiments, verifying the performance of the nanoprobe and offer its possibilities to other research groups. Based on the experiences with that prototype, the beamline ID 13 has implemented its own nanoprobe setup, for which we provided an interface module in order to mount NFLs developed by our research group in Dresden.

The remainder of this document is organized as follows. Chapter 2 gives a general introduction to the properties of hard x rays, dealing with the subject of free-space propagation and the interaction of x rays with matter. The properties of x-ray sources are discussed in chapter 3. After identifying the demands on the source, the most important characteristics of synchrotron radiation produced by undulators are highlighted. Focusing x-ray optics are treated in chapter 4. Besides NFLs and CRLs, which are the core of the scanning microscope, I also touch on adiabatically focusing lenses (AFLs). The basic properties of the nano beam, which is generated by NFLs, are discussed, and a two-stage focusing scheme is presented. The conceptual design and the realization of the hard x-ray scanning microscope are given in chapter 5. The layout of the ESRF beamline ID 13 is shown as well as the hardware components of the instrument, including optics, stages, and detectors. Finally, in chapter 6 a selection of experiments will give evidence of the performance of the hard x-ray scanning microscope. This work is completed by a conclusion and an outlook on prospective plans in implementing an improved version of the prototype instrument.

# Chapter 2

# Basic Properties of Hard X Rays

Like visible light, x-ray radiation is part of the electromagnetic spectrum but with a wavelength much shorter than that of visible light. Whereas the wavelength of visible light is in the range between 380 nm snd 780 nm, the wavelength of x rays is shorter than 1 nm. The corresponding photon energies $E_{ph} = hc_0/\lambda$ ($h$ the Planck number, $c_0$ the speed of light in vacuum) are in the order of 1 eV for visible light, but higher than 200 eV for x rays. As a common convention, there is the distinction between soft x rays with photon energies of several 100 eV up to about several keV on the one hand, and hard x rays with photon energies larger than a few keV on the other hand. In contrast to hard x rays, soft x rays do not penetrate very deeply into matter, they are even absorbed significantly in the air for short propagation distances. The phenomenological difference between the properties of soft and hard x rays is quite significant, the experimental handling of soft x rays as well as their potential applications are much different from that of hard x rays and, therefore, different scientific communities for soft x-ray physics and hard x-ray physics have emerged. The scanning microscope treated in this thesis is intended to be employed for hard x rays, allowing to investigate the inner structure of objects. For this reason, the emphasis is laid on hard x rays, even though some of the properties discussed in this chapter are also valid for soft x rays.

## 2.1 Free Propagation of X Rays

In the scanning microscope x rays propagate from the source to several optical elements, then they propagate to the sample (which hopefully is located in the focal plane of the focusing lens), and finally — after interacting with the sample — x rays propagate from the sample to the detector. Obviously, knowledge about free propagation of x rays is critical in order to understand the scanning microscope. In this section, I provide the theoretical basis that is needed to quantitively treat the propagation of light, and consequently of hard x rays.

The question to be treated in this section will be the following. Given the electromagnetic field amplitudes of the x rays within a certain plane perpendicular to the optical axis, what are the field amplitudes within a plane at some distance further in the direction of

propagation, if there is only free space between the two planes? This question will be answered by classic electrodynamics, using Maxwell's equations. In a first step I will introduce the Helmholtz equation, a scalar wave function for monochromatic waves. The Helmholtz equation will be used to deduce the integral theorem of Helmholtz and Kirchhoff, which will be adapted to a physical situation which conforms with the needs of simulating free propagation of x rays in the scanning microscope, leading to the Fresnel-Kirchhoff diffraction formula. In a last step I will discuss some approximations being of special relevance in practical situations.

### 2.1.1 The Helmholtz Equation

We start with Maxwell's equations

$$\begin{aligned} \frac{\partial}{\partial \boldsymbol{r}} \times \boldsymbol{E}(\boldsymbol{r},t) &= -\frac{\partial}{\partial t}\boldsymbol{B}(\boldsymbol{r},t), && (2.1)\\ \frac{\partial}{\partial \boldsymbol{r}}\,\boldsymbol{E}(\boldsymbol{r},t) &= \frac{1}{\epsilon_0}\rho(\boldsymbol{r},t), && (2.2)\\ \frac{\partial}{\partial \boldsymbol{r}} \times \boldsymbol{B}(\boldsymbol{r},t) &= \mu_0\,\boldsymbol{j}(\boldsymbol{r},t) + \epsilon_0\,\mu_0\,\frac{\partial}{\partial t}\boldsymbol{E}(\boldsymbol{r},t), && (2.3)\\ \frac{\partial}{\partial \boldsymbol{r}}\,\boldsymbol{B}(\boldsymbol{r},t) &= 0. && (2.4) \end{aligned}$$

This set of partial differential equations describes the fields $\boldsymbol{E}(\boldsymbol{r},t)$ and $\boldsymbol{B}(\boldsymbol{r},t)$ and forms the fundament of classic electrodynamics. Applying some mathematical manipulations on these equations leads to wave equations for the electromagnetic fields. With $1/c^2 = \mu_0\epsilon_0$ the wave equations read

$$\begin{aligned} \frac{\partial^2}{\partial \boldsymbol{r}^2}\boldsymbol{E} - \frac{1}{c^2}\frac{\partial^2}{\partial t^2}\boldsymbol{E} &= \frac{1}{\epsilon_0}\frac{\partial}{\partial \boldsymbol{r}}\rho + \mu_0\frac{\partial}{\partial t}\boldsymbol{j},\\ \frac{\partial^2}{\partial \boldsymbol{r}^2}\boldsymbol{B} - \frac{1}{c^2}\frac{\partial^2}{\partial t^2}\boldsymbol{B} &= -\mu_0\frac{\partial}{\partial \boldsymbol{r}} \times \boldsymbol{j}. && (2.5) \end{aligned}$$

If we consider a region far away from any charged particles, the charge density $\rho$ and the current density $\boldsymbol{j}$ are zero and the inhomogeneous wave equations become homogeneous

$$\begin{aligned} \frac{\partial^2}{\partial \boldsymbol{r}^2}\boldsymbol{E} - \frac{1}{c^2}\frac{\partial^2}{\partial t^2}\boldsymbol{E} &= 0,\\ \frac{\partial^2}{\partial \boldsymbol{r}^2}\boldsymbol{B} - \frac{1}{c^2}\frac{\partial^2}{\partial t^2}\boldsymbol{B} &= 0. && (2.6) \end{aligned}$$

It can be shown that *plane waves*

$$\begin{aligned} \boldsymbol{E}(\boldsymbol{r},t) &= \boldsymbol{E}_0\, f(\boldsymbol{n}\boldsymbol{r} - ct),\\ \boldsymbol{B}(\boldsymbol{r},t) &= \boldsymbol{B}_0\, f(\boldsymbol{n}\boldsymbol{r} - ct) && (2.7) \end{aligned}$$

with $|\boldsymbol{n}| = 1$ are valid solutions of the wave equations. For each given point in time the field values are constant over planes orthogonal to $\boldsymbol{n}$. These planes of constant field values propagate in time along the direction given by $\boldsymbol{n}$. Since we consider regions free of electric charges ($\rho = 0$), it follows from equations (2.2) and (2.4) that

$$\begin{aligned} \boldsymbol{n}\boldsymbol{E} &= 0, \\ \boldsymbol{n}\boldsymbol{B} &= 0 \end{aligned}$$

and, therefore, the field vectors $\boldsymbol{E}$ and $\boldsymbol{B}$ are both orthogonal to the direction of propagation. Furthermore, on applying equation (2.1), the expression

$$\boldsymbol{n}\frac{\partial}{\partial \boldsymbol{r}} \times \boldsymbol{E}_0 = c\boldsymbol{B}_0 \tag{2.8}$$

can be deduced, showing that the three vectors $\boldsymbol{n}$, $\boldsymbol{E}$ and $\boldsymbol{B}$ are all perpendicular to each other and form in this order an orthogonal right-handed tripod. If one neglects polarization effects, the electric and the magnetic field amplitudes maybe written in a scalar form. Following the convention in [BW99], I use $V(\boldsymbol{r}, t)$ to represent the scalar electric field amplitude. This is possible without loss of information, since equation (2.8) allows to determine the magnetic field, once the electric field is known, or vice versa.

A special class of solutions of the homogeneous wave equation (2.6) is that for which the space-dependence separates from the time-dependence, i. e., which can be written in the form

$$V(\boldsymbol{r}, t) = U(\boldsymbol{r})\, T(t). \tag{2.9}$$

Inserting this ansatz into (2.6) one retrieves

$$\left(\frac{\partial^2}{\partial \boldsymbol{r}^2} + k^2\right) U(\boldsymbol{r}) = 0, \tag{2.10}$$

$$\left(\frac{\partial^2}{\partial t^2} + k^2/c^2\right) T(t) = 0. \tag{2.11}$$

Equation (2.11) has time harmonic solutions

$$T(t) = T_0\, e^{\mathrm{i}\omega t} \tag{2.12}$$

with $\omega = k/c$. The time-independent wave equation (2.10) is called *Helmholtz equation* and delivers solutions $U_\omega(\boldsymbol{r})$, which, together with (2.12), solve equation (2.9)

$$V_\omega(\boldsymbol{r}, t) = T_0\, e^{\mathrm{i}\omega t}\, U_\omega(\boldsymbol{r}). \tag{2.13}$$

If $U_\omega(\boldsymbol{r})$ solves the Helmholtz equation (2.10), then $T_0\, U_\omega(\boldsymbol{r})$ is also a solution and, therefore, instead of (2.13), one can also write

$$V_\omega(\boldsymbol{r}, t) = U_\omega(\boldsymbol{r})\, e^{\mathrm{i}\omega t}. \tag{2.14}$$

These solutions are called monochromatic waves, and each general solution of the general homogeneous wave equation (2.6) can be written as a linear superposition of such monochromatic waves

$$\begin{aligned} V(\boldsymbol{r},t) &= \int d\omega\, V_\omega(\boldsymbol{r},t) \\ &= \int d\omega\, U_\omega(\boldsymbol{r})\, e^{\mathrm{i}\,\omega\, t}. \end{aligned} \tag{2.15}$$

To go a step forward, we display $U_\omega(\boldsymbol{r})$ as a linear combination of plane waves

$$V(\boldsymbol{r},t) = \int d\omega \int d^3\boldsymbol{k}\, \tilde{U}_{\boldsymbol{k},\omega}\, e^{\mathrm{i}\,\boldsymbol{k}\,\boldsymbol{r}}\, e^{\mathrm{i}\,\omega\, t}. \tag{2.16}$$

In order to be a solution of (2.6), the relation $k = |\boldsymbol{k}| = \omega/c$ is required, and after integration over $d\omega$ one obtains

$$V(\boldsymbol{r},t) = \int d^3\boldsymbol{k}\, \left(\tilde{U}_1(\boldsymbol{k})\, e^{\mathrm{i}(\,\boldsymbol{k}\,\boldsymbol{r} - c\,k\,t)} + \tilde{U}_2(\boldsymbol{k})\, e^{\mathrm{i}(\,\boldsymbol{k}\,\boldsymbol{r} + c\,k\,t)}\right) \tag{2.17}$$

with $k = |\boldsymbol{k}|$. From these considerations it becomes obvious, that the Helmholtz equation (2.10), together with appropriate boundary conditions, completely describes the propagation of x rays in vacuum.

### 2.1.2 Integral Theorem of Helmholtz and Kirchhoff

Now, we will apply the Helmholtz equation to calculate the amplitude $U(P_0)$ of the x-ray field in a point $P_0 = \boldsymbol{r}_0$ with the assumption that the amplitude and its derivative are known on an arbitrary surface $S$ which surrounds the point $P_0$ (Figure 2.1). We start with a small sphere $S_\epsilon$ with radius $\epsilon$ centered around $P_0$ and examine the following integral

$$I_{S_\epsilon} = \iint\limits_{S_\epsilon} d\boldsymbol{s}\, \left(U(\boldsymbol{s})\, \frac{\partial G(\boldsymbol{s})}{\partial n} - G(\boldsymbol{s})\, \frac{\partial U(\boldsymbol{s})}{\partial n}\right) \tag{2.18}$$

with

$$G(\boldsymbol{s}) = \frac{e^{ik_0 r(\boldsymbol{s})}}{r(\boldsymbol{s})}. \tag{2.19}$$

$r(\boldsymbol{s}) = |\boldsymbol{s} - \boldsymbol{r}_0|$ is the distance from the observation point $P_0$, and $\partial/\partial n = \boldsymbol{n}\boldsymbol{\partial}$ denotes the directional derivative along the inward facing surface normal $\boldsymbol{n}$. We evaluate the integral for the limit $\epsilon \to 0$

$$\begin{aligned} I_{S_\epsilon} &= \iint\limits_{S_\epsilon} d\boldsymbol{s}\, \left(-U(\boldsymbol{s})\, \left[\frac{1}{\epsilon} - ik_0\right] \frac{e^{ik_0\epsilon}}{\epsilon} - \frac{e^{ik_0\epsilon}}{\epsilon}\, \frac{\partial U(\boldsymbol{s})}{\partial n}\right) \\ &= e^{ik_0\epsilon} \left[\int_{\phi=0}^{2\pi} d\phi \int_{\theta=0}^{\pi} d\theta \sin\theta\, (-U + \epsilon\, i\, k_0\, U - \epsilon\, \boldsymbol{n}\, \boldsymbol{\partial} U)\right] \\ &= -4\pi\, U(P_0) \quad \text{as} \quad \epsilon \to 0 \end{aligned}$$

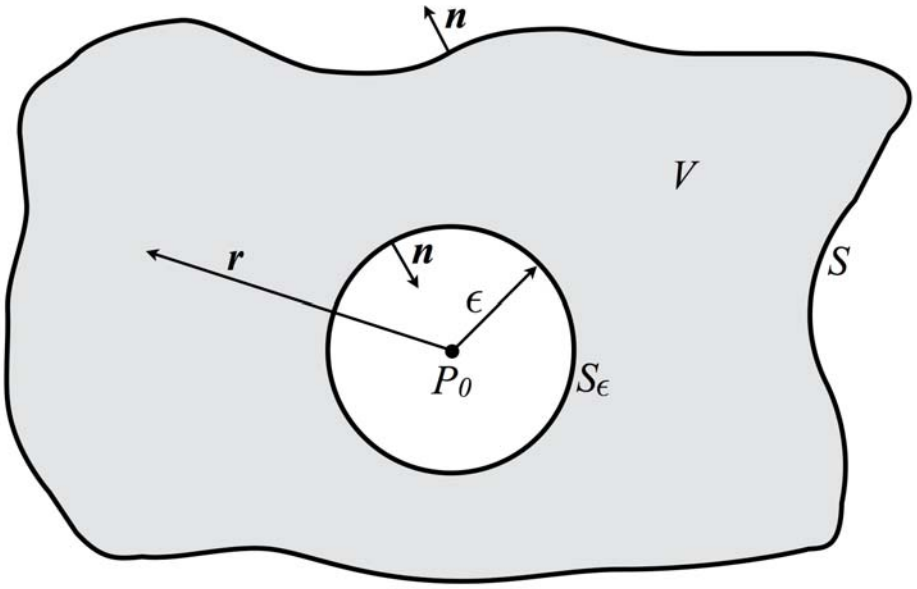


Figure 2.1: Derivation of the Integral Theorem of Helmholtz and Kirchhoff. The field $U$ is known on the surface $S$. Since $U$ is a solution of the Helmholtz equation, the field on the surface $S_\epsilon$ is completely determined by the field on $S$. Computing the limit for $\epsilon \to 0$, the field amplitude in the observation point $P_0$ can be deduced.

and thus

$$U(P_0) = \frac{1}{4\pi} \iint_{S_\epsilon} d\boldsymbol{s} \left( G \frac{\partial U}{\partial n} - U \frac{\partial G}{\partial n} \right). \tag{2.20}$$

This expression relates the field amplitude $U(P_0)$ observed at location $P_0$ with the integral over the infinitesimal spherical surface $S_\epsilon$ around $P_0$. Now we use Green's theorem together with the Helmoltz equation to connect the field amplitude at the observation point $P_0$ with the field on the surface $S$. In contrast to $S_\epsilon$ the surface $S$ needs neither to be spherical nor to be infinitesimal small. Shall $V$ denote the volume which is surrounded from outside by the surface $S$ and from inside by the surface $S_\epsilon$. If the partial derivatives of the functions $U$ and $G$ exist and are continuous everywhere on $S$, on $S_\epsilon$, and within the volume $V$, then Green's theorem states

$$\iint\limits_{S \cup S_\epsilon} d\boldsymbol{s} \left( G \frac{\partial U}{\partial n} - U \frac{\partial G}{\partial n} \right) = \iiint\limits_{V} d\boldsymbol{v} \left( G \frac{\partial^2}{\partial \boldsymbol{r}^2} U - U \frac{\partial^2}{\partial \boldsymbol{r}^2} G \right) \tag{2.21}$$

Here, the surface normal $\boldsymbol{n}$ is chosen to face away from the volume $V$, which conforms with the convention used in the derivation of (2.20). The function $G = \exp(ik_0 r)/r$ has been chosen such that it is a solution of the Helmholtz equation (2.10) with the wave number

$k = k_0$. If $U$ satisfies the Helmholtz equation with the same wave number $k_0$, i. e.,

$$\begin{aligned} \frac{\partial^2}{\partial \boldsymbol{r}^2} U &= -k_0^2\, U, \\ \frac{\partial^2}{\partial \boldsymbol{r}^2} G &= -k_0^2\, G, \end{aligned}$$

then the integrand of the volume integral vanishes and Green's theorem (2.21) simplifies to

$$\iint\limits_{S \cup S_\epsilon} d\boldsymbol{s} \left( G \frac{\partial U}{\partial n} - U \frac{\partial G}{\partial n} \right) = 0$$

or

$$\iint\limits_{S_\epsilon} d\boldsymbol{s} \left( G \frac{\partial U}{\partial n} - U \frac{\partial G}{\partial n} \right) = \iint\limits_{S} d\boldsymbol{s} \left( U \frac{\partial G}{\partial n} - G \frac{\partial U}{\partial n} \right).$$

This expression can be inserted into equation (2.20), and finally one gets the relation between the wave field on the surface $S$ and the amplitude at the observed point $P_0$

$$U(P_0) = \frac{1}{4\pi} \iint\limits_{S} d\boldsymbol{s} \left( U \frac{\partial}{\partial n} G - G \frac{\partial U}{\partial n} \right) \tag{2.22}$$

with

$$G = \frac{e^{i\, k_0\, r}}{r}. \tag{2.23}$$

This formula is a special version of the integral theorem of Helmholtz and Kirchhoff and will be used in the next subsection to derive Fresnel-Kirchhoff's diffraction formula.

### 2.1.3 Fresnel-Kirchhoff's Diffraction Formula

In the preceding subsection the integral theorem of Helmholtz and Kirchhoff was presented. This theorem admits the calculation of the scalar field amplitude in an observation point from the knowledge of the field and its derivatives on a surface which encloses this point. Now, we will apply this theorem to manage the following situation, which is illustrated in Figure 2.2. X rays, which have been emitted from a source, are propagating from the left to the right along the optical axis and arrive at an open aperture within an opaque screen. The source distance shall be large compared to the transverse dimensions of the open aperture. Knowing the wave field in the aperture plane, one would like to estimate the field amplitude $U(P_0)$ in a point $P_0$ behind the aperture plane. In order to apply the integral theorem from the previous subsection, we introduce an imaginary surface $S$, which encloses $P_0$ as shown in Figure 2.2. The enclosing surface shall be composed of three disjoint parts $S_1$, $S_2$ and $S_3$ with $S_1$ matching the opening aperture, $S_2$ conforming a part of the opaque screen and $S_3$ being the surface of a large sphere with radius $R$ centered around $P_0$ and cutting the opaque

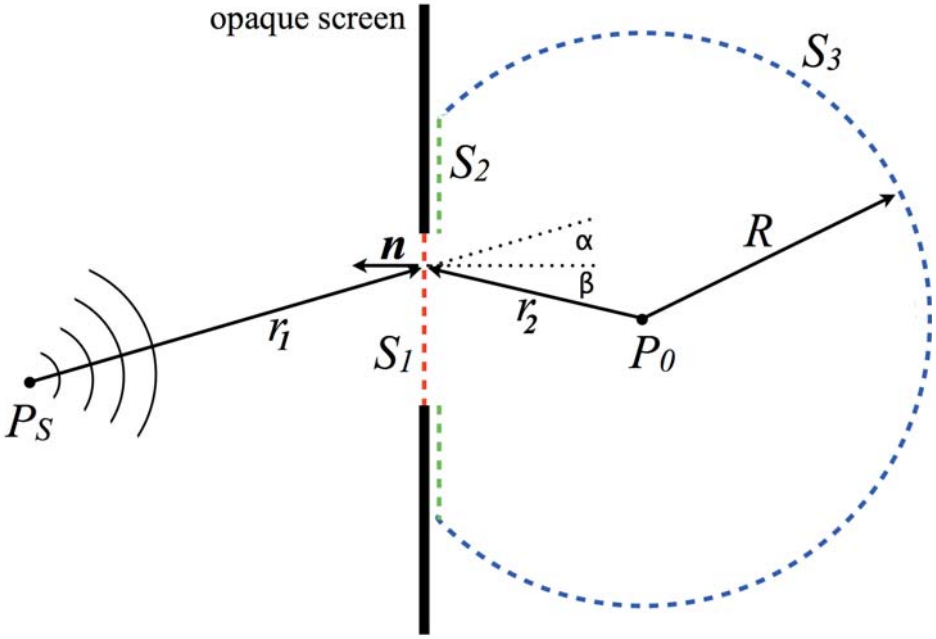


Figure 2.2: Illustrating the derivation of Fresnel-Kirchhoff's Diffraction Formula. A source radiates a wavefield which propagates to an opaque screen with an open aperture $S_1$. Knowing the wavefield on $S_1$ is sufficient to compute the amplitude in the observation point $P_0$, because the contributions from $S_2$ and $S_3$ can be neglected.

screen in a way that the opening aperture lies within the cutting circle. Due to (2.22) it follows for the field amplitude in $P_0$

$$\begin{aligned} U(P_0) &= \frac{1}{4\pi} \iint\limits_{S_1 \cup S_2 \cup S_3} d\boldsymbol{s} \left( U \frac{\partial}{\partial n} G - G \frac{\partial U}{\partial n} \right) \\ &= \sum_{i \in \{1,2,3\}} U_i \end{aligned} \tag{2.24}$$

with

$$U_i = \frac{1}{4\pi} \iint\limits_{S_i} d\boldsymbol{s} \left( U \frac{\partial}{\partial n} G - G \frac{\partial U}{\partial n} \right), \quad i \in \{1,2,3\}. \tag{2.25}$$

The contributions from the three surfaces $S_i$ can be evaluated separately, but it will be necessary to establish some boundary conditions for the field and its derivative on these surfaces. For the open aperture $S_1$ it is reasonable to assume that $U$ and its derivative should be the same as without the opaque screen around, even though there may be some deviations near the edge of the aperture. The influence of the field, that is generated by the illuminated opaque screen, on the field in the aperture $S_1$, is very low and can be neglected, which is especially true for the hard x-ray regime of the electromagnetic spectrum. In the shadow just behind the opaque screen the field and its derivative can be expected to be zero,

since the opaque screen absorbs all illuminating radiation, and again, the influence of the field, which is generated by the presence of the screen, can be neglected in comparison with the incident wavefront. It remains to show that the field and its derivatives on the spheric surface $S_3$ vanish for a radius $R$ which is sufficiently large. The argumentat is not as obvious as it seems, because, even if the field $U$ falls with increasing radius, the area of $S_3$ increases beyond all limits and the contribution of $U_3$ would not vanish. Instead, as suggested in [BW99], one can presume that the source of the incident wavefront has been switched on at a certain point in time $t_0$ and that there was no electromagnetic field before. Thus, at the time $t_1$ for which we evaluate the amplitude in $P_0$, no photon has reached $S_3$ if only the radius $R$ is sufficiently large ($R > c(t_1 - t_0)$). Of course this argumentation contradicts with the use of the Helmholtz equation which assumes a stationary situation with strictly monochromatic waves. A more rigorous argumentation avoiding this difficulty can be found in [Bor06] or [BC03]. As a summary, the following boundary conditions are encountered:

- on $S_1$: $U = U^{(i)}$, $\frac{\partial U}{\partial n} = \frac{\partial U^{(i)}}{\partial n}$,
- on $S_2$: $U = 0$, $\frac{\partial U}{\partial n} = 0$,
- on $S_3$: $U = 0$, $\frac{\partial U}{\partial n} = 0$,

from which it follows that $U_2$ and $U_3$ do not contribute to the amplitude $U(P_0)$ and, therefore,

$$U(P_0) = U_1 = \frac{1}{4\pi} \iint\limits_{S_1} d\boldsymbol{s} \left( U \frac{\partial}{\partial n} G - G \frac{\partial U}{\partial n} \right).$$

The Green function $G$ is given by (2.23) and the wavefront $U$ must obey the Helmholtz equation with the wavenumber $k_0$. I start with a special solution given by a spherical wave emitted from a point source at $P_S$ and deduce the general case by a linear superposition of many spherical wavelets. With

$$\begin{aligned} U &= U_0 \frac{e^{ik_0 r_1}}{r_1}, \\ G &= \frac{e^{ik_0 r_2}}{r_2} \end{aligned} \tag{2.26}$$

one gets

$$\begin{aligned} U(P_0) &= \frac{1}{4\pi} \iint\limits_{S_1} d\boldsymbol{s} \left( U_0 \frac{e^{ik_0 r_1}}{r_1} \frac{\partial}{\partial n} \frac{e^{ik_0 r_2}}{r_2} - \frac{e^{ik_0 r_2}}{r_2} \frac{\partial U_0 \frac{e^{ik_0 r_1}}{r_1}}{\partial n} \right) \\ &= \frac{1}{4\pi} \iint\limits_{S_1} d\boldsymbol{s}\ U_0 \frac{e^{ik_0 (r_1 + r_2)}}{r_1\, r_2} \left( \left[ ik_0 \cos\beta + \frac{1}{r_2} \right] + \left[ ik_0 \cos\alpha + \frac{1}{r_1} \right] \right) \\ &= \frac{1}{4\pi} \iint\limits_{S_1} d\boldsymbol{s}\ U(r_1)\, G(r_2) \left( ik_0 \left[ \cos\alpha + \cos\beta \right] + \frac{1}{r_1} + \frac{1}{r_2} \right). \end{aligned}$$